Modulation of Human 5-Lipoxygenase Activity by Membrane Lipids†

Abhay H. Pande,‡ David Moe,‡ Kathleen N. Nemec, Shan Qin, Shuhua Tan, and Suren A. Tatulian*

Biomolecular Science Center, University of Central Florida, Orlando, Florida 32826

Received June 11, 2004; Revised Manuscript Received September 9, 2004

ABSTRACT: Mammalian 5-lipoxygenase (5-LO) catalyzes the conversion of arachidonic acid (AA) to leukotrienes, potent inflammatory mediators. 5-LO is activated by a Ca^{2+}-mediated translocation to membranes, and demonstrates the characteristic features of interfacially activated enzymes, yet the mechanism of membrane binding of 5-LO is not well understood. In an attempt to understand the mechanism of lipid-mediated activation of 5-LO, we have studied the effects of a large set of lipids on human recombinant 5-LO activity, as well as mutual structural effects of 5-LO and membranes. In the presence of 0.35 mM phosphatidylcholine (PC) and 0.2 mM Ca^{2+}, there was substrate inhibition at >100 μM AA. Data analysis at low AA concentrations yielded the following: $K_m \approx 103\ \mu M$ and $k_{cat} \approx 56\ s^{-1}$. 5-LO activity was supported by PC more than by any other lipid tested except for a cationic lipid, which was more stimulatory than PC. Binding of 5-LO to zwitterionic and acidic membranes was relatively weak; the extent of binding increased 4−8 times in the presence of Ca^{2+}, whereas binding to cationic membranes was stronger and essentially Ca^{2+}-independent. Polarized attenuated total reflection infrared experiments implied that 5-LO binds to membranes at a defined orientation with the symmetry axis of the putative N-terminal β-barrel tilted ~45° from the membrane normal. Furthermore, membrane binding of 5-LO resulted in dehydration of the membrane surface and was paralleled with stabilization of the structures of both 5-LO and the membrane. Our results provide insight into the understanding of the effects of membrane surface properties on 5-LO−membrane interactions and the interfacial activation of 5-LO.

Enzymes of the lipoxygenase (LO)[1] family are found in animals, higher plants, and fungi, where they catalyze oxygenation of polyunsaturated fatty acids and thus initiate the biosynthesis of bioactive mediators, such as leukotrienes and lipoxins in animals and jasmonic acid in plants (*1*−*6*). Mammalian 5-lipoxygenase (5-LO) is particularly important because of its unique ability to convert arachidonic acid (AA) to 5-hydroperoxyeicosatetraenoic acid (5-HPETE) and then to leukotriene A_4 (LTA_4), a key intermediate in biosynthesis of all leukotrienes that act as potent mediators of allergy, inflammation, apoptosis, and tumorigenesis (*2*, *7*−*15*).

LOs are non-heme enzymes, which contain a single iron cofactor coordinated by a number of histidines and the carboxyl group of the C-terminal isoleucine. Currently, the atomic-resolution structures of soybean LO isoforms 1 and 3 and the rabbit reticulocyte 15-lipoxygenase (15-LO) are available. X-ray crystal structures of soybean and rabbit LOs revealed two major structural domains, an N-terminal eight-stranded β-barrel domain and a larger, mostly α-helical catalytic domain that contains the iron site (*16*−*20*). Although the structure of 5-LO has not been determined, this enzyme is believed to share major structural features of rabbit 15-LO, including the N-terminal β-barrel, because the sequences of these proteins are 37% identical and 57% similar.

There is strong evidence that 5-LO is activated upon cell stimulation via a Ca^{2+}-mediated binding to nuclear membranes (*21*−*30*), yet the reason for specific localization of 5-LO to the nuclear membranes, as well as the mechanism of membrane binding and activation of 5-LO, is unclear (*7*, *9*, *31*). We have shown previously that soybean lipoxygenase-1 undergoes a functionally important, Ca^{2+}-mediated membrane binding, and the N-terminal β-barrel domain was suggested to act as a C2-like domain to facilitate membrane binding (*32*). Later, studies on the truncated and full-length human 5-LO, including site-directed mutagenesis and membrane binding experiments, identified the N-terminal domain

† This work was supported, in part, by National Institutes of Health Grant HL65524.

* To whom correspondence should be addressed. Telephone: (407) 882-2260. Fax: (407) 384-2062. E-mail: statulia@mail.ucf.edu.

‡ These authors contributed equally to this work.

[1] Abbreviations: 15-LO, 15-lipoxygenase; 5-HPETE, 5-hydroperoxyeicosatetraenoic acid; 5-LO, 5-lipoxygenase; AA, arachidonic acid; CD, circular dichroism; CL, cardiolipin; DAG, diacylglycerol; DMEPC, 1,2-dimyristoyl-*sn*-glycero-3-ethylphosphocholine; DPPC, 1,2-dipalmitoyl-*sn*-glycero-3-phosphocholine; FLAP, 5-lipoxygenase activating protein; GP, generalized polarization; Laurdan, 6-lauroyl-2-(*N*,*N*-dimethylamino)naphthalene; LO, lipoxygenase; LTA_4, leukotriene A_4; Lyso-PA, 1-oleoyl-2-hydroxy-*sn*-glycero-3-phosphate (sodium salt); Lyso-PC, 1-oleoyl-2-hydroxy-*sn*-glycero-3-phosphocholine; PA, phosphatidic acid; PC, phosphatidylcholine; PG, phosphatidylglycerol; PI, L-α-phosphatidylinositol (sodium salt); PIP, L-α-phosphatidylinositol 4-phosphate (diammonium salt); PIP_2, L-α-phosphatidylinositol 4,5-bisphosphate (triammonium salt); POG, 1-palmitoyl-2-oleoyl-*sn*-glycerol; POPA, 1-palmitoyl-2-oleoyl-*sn*-glycero-3-phosphate (sodium salt); POPC, 1-palmitoyl-2-oleoyl-*sn*-glycero-3-phosphocholine; POPE, 1-palmitoyl-2-oleoyl-*sn*-glycero-3-phosphoethanolamine; POPG, 1-palmitoyl-2-oleoyl-*sn*-glycero-3-phosphoglycerol (sodium salt); POPS, 1-palmitoyl-2-oleoyl-*sn*-glycero-3-phosphoserine (sodium salt); PS, phosphatidylserine; Py-PE, 1,2-dioleoyl-*sn*-glycero-3-phosphoethanolamine-*N*-(1-pyrenesulfonyl); RET, resonance energy transfer; SDS−PAGE, sodium dodecyl sulfate−polyacrylamide gel electrophoresis; TBST, buffer containing 137 mM NaCl, 0.1% Tween 20, and 20 mM Tris-HCl (pH 7.6).

10.1021/bi048775y CCC: $27.50 © 2004 American Chemical Society
Published on Web 10/30/2004

of 5-LO as a determinant of Ca^{2+}-dependent membrane binding of the enzyme (*33*−*35*). These results, along with similar findings about other LO isoforms, led to a general recognition that the N-terminal domains of mammalian and plant LOs may function as C2 domains to facilitate their Ca^{2+}-mediated membrane binding (*33*−*39*).

Localization of 5-LO to the nuclear membrane might be influenced either by specific interactions between 5-LO and nuclear membrane proteins or lipids or by nonspecific factors such as membrane surface charge or the distinct lipid composition of the nuclear membrane. In fact, nuclear membranes of cells producing leukotrienes comprise an integral protein, 5-lipoxygenase activating protein (FLAP), which significantly increases both hydroperoxidase and LTA_4 synthetase activities of 5-LO (*30*, *40*, *41*). However, the fact that 5-LO binding to nuclear membranes is FLAP-independent (*9*, *26*) and the fact that artificial lipid membranes or neutrophil plasma membranes are able to activate 5-LO in the absence of FLAP (*42*−*45*) strongly imply that FLAP is not a molecular determinant for nuclear membrane localization of 5-LO. This raises the possibility that the specific lipid composition of nuclear membranes may influence the subcellular localization of 5-LO.

To date, a limited number of lipids have been examined in terms of 5-LO binding and supporting the enzyme activity, including phosphatidylcholine (PC), phosphatidylethanolamine (PE), phosphatidylserine (PS), phosphatidylglycerol (PG), phosphatidylinositol (PI), and diacylglycerol (DAG) (*35*, *42*, *43*). The putative C2-like domain of 5-LO, as well as the full-length enzyme, was shown to bind to pure PC membranes more strongly than to membranes containing acidic lipids, such as PG or PS, and PC turned out to support 5-LO activity much better than other lipids that were tested (*35*, *42*, *43*). Although 5-LO was shown to undergo Ca^{2+}-mediated binding to PE, and to a somewhat lesser extent to PS membranes (*43*), these lipids were found to be poor 5-LO activators (*42*), implying that not only the membrane binding strength but also the productive-mode orientation at the membrane surface is probably important for 5-LO function.

Despite the important role of lipid membranes in 5-LO function, the dependence of 5-LO activity on specific lipid composition of membranes has not been broadly studied, nor has the interaction of 5-LO with membranes with various lipid compositions been quantitatively described. In this work, we examine the dependence of 5-LO activity on 17 different lipids commonly occurring in intracellular membranes. Acidic lipids inhibit 5-LO activity, while a cationic lipid enhances 5-LO activity 2-fold. There is no simple correlation between membrane surface charge and 5-LO activity, however, implying that specific 5-LO−lipid interactions also play a role. Quantitative membrane binding experiments show that binding of 5-LO to zwitterionic and acidic membranes is weak in the absence of Ca^{2+} and is strengthened 4−8 times by 0.2 mM Ca^{2+}, whereas binding to cationic membranes is ~20-fold stronger and essentially Ca^{2+}-independent. By attenuated total reflection Fourier transform infrared (ATR-FTIR) spectroscopy, we characterize the kinetics of membrane binding of 5-LO and show that (i) the enzyme binds to the membrane at a defined orientation, (ii) membrane binding of 5-LO causes dehydration of the membrane surface, and (iii) the structures of both membrane lipids and 5-LO become more stable upon their interaction.

EXPERIMENTAL PROCEDURES

Materials. Expression vector pET-21 was purchased from Novagen (Madison, WI), and the pGem-T vector was from Promega (Madison, WI). T4 ligase was from USB Corp. (Cleveland, OH). *Nde*I and *Hin*dII restriction endonucleases were from New England Biolabs (Mississauga, ON), and carbenicillin, lysozyme, casamino acids, and protease inhibitor cocktail were from Sigma (St. Louis, MO). Arachidonic acid and anti-human 5-LO antibody were from Cayman Chemical Co. (Ann Arbor, MI). All lipids were purchased from Avanti Polar Lipids, Inc. (Alabaster, AL), and originated from the following sources. PI was purified from bovine liver. PI mono- and bis-phosphates, as well as ceramide, cerebroside and sphingomyelin, were purified from porcine brain. Cholesterol was from egg yolk, and all other lipids were synthetic. Most of the chemicals were purchased from Sigma, and the sources of other supplies are specified.

Expression and Purification of 5-LO. The 5-LO plasmid, pT3-5LO, was kindly provided by Y.-Y. Zhang (Boston University School of Medicine, Boston, MA) and has been described by Zhang et al. (*46*). The 5-LO open reading frame was placed into the pET-21 expression vector using directional cloning. PCR amplification was carried out with primers 5′-GCAATTCCATATGCCCTCCTACACG-3′ and 5′-CCCAAGCTTTCAGATGGCCACACTGTT-3′, which were designed using Primer Select (Lasergene). The PCR product was first placed into the pGem-T vector and the sequence confirmed (Beckman-Coulter CEQ) before subcloning into pET-21. Subcloning was achieved using the *Nde*I and *Hin*dIII sites designed as part of the primers. The insert (5-LO) and pET-21 were doubly digested by *Nde*I and *Hin*dIII, followed by purification from a 1% agarose gel using the gel extraction kit (Qiagen) and ligation using a T4 ligase. Ligated products were electroporated into DH5α, and the sequence was confirmed. Positive clones were placed in *Escherichia coli* strain BL21-DE3 for T7-driven expression.

A 50 mL culture of transformed BL21-DE3 cells was grown overnight in LB medium, supplemented with 0.1 mg/mL carbenicillin, and diluted into 1 L of M9CA medium (42 mM Na_2HPO_4, 24 mM KH_2PO_4, 9 mM NaCl, 19 mM NH_4Cl, 1 mM $MgSO_4$, 0.1 mM $CaCl_2$, 0.2% D-glucose, 0.1% casamino acids, 5 μM $FeSO_4$, and 0.1 mg/mL carbenicillin). The culture was gown at 25 °C and induced with 0.25 mM IPTG at an OD_{600} of ≈0.6. When the culture reached an OD_{600} of ~2.0 (16−20 h postinduction at 25 °C), the cells were pelleted at 5000*g* for 10 min and resuspended in buffer A [10 mM β-mercaptoethanol, 0.1 mM EDTA, and 50 mM triethanolamine (pH 7.3)] supplemented with a protease inhibitor cocktail and 0.5 mg/mL lysozyme. After being stirred on ice for 30 min, cells were sonicated twice, for 1 min each time. The cell lysate was cleared by being spun for 15 min at 15000*g*. Proteins in the supernatant were precipitated with 50% saturated $(NH_4)_2SO_4$ and spun at 16000*g* for 15 min. Proteins in the salt pellet can then be stored at −80 °C without a considerable loss of 5-LO activity for several months (*47*). The salt pellet from 1 L of culture was resuspended in 25 mL of buffer A and cleared by being spun at 40000*g* for 15 min and passed through a 0.22 μm

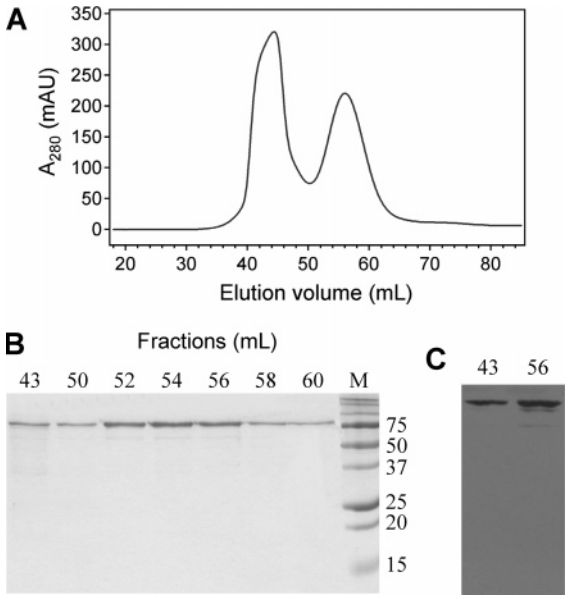

FIGURE 1: Final steps of 5-LO purification and identification. (A) The profile of elution of 5-LO from a HiLoad Superdex-75 size-exclusion column shows two well-resolved protein peaks. (B) SDS−PAGE indicates that both elution peaks contain a pure $M_r \approx 78$ kDa protein. (C) Western blot analysis of two protein peaks identifies the protein in both peaks as 5-LO.

polyethersulfone filter (Nalgene). All buffers used for 5-LO purification were extensively degassed to remove oxygen, which is known to cause 5-LO inactivation. The 5-LO sample was loaded onto a 6 mL ATP−agarose column (Sigma) for affinity purification, using an Äkta purifier (Amersham). The column was washed with 1 column volume of a gradient between buffer A and the same buffer supplemented with 1 M NaCl to remove nonspecifically bound proteins. 5-LO bound to the ATP−agarose column was then eluted at 0.1 mL/min with buffer A containing 100 mM NaCl and 12 mM ATP. The first two column volumes of the elution contained a protein peak mainly comprised of 5-LO. Sodium dodecyl sulfate−polyacrylamide gel electrophoresis (SDS−PAGE) of these fractions showed a major band at ∼78 kDa, in addition to several smaller proteins. These fractions were prepared for size-exclusion chromatography by being passed through a 5 mL HiTrap G-25 desalting column (Amersham) to place the sample in buffer B [1 M NaCl, 0.1 mM EDTA, and 50 mM Tris-HCl (pH 7.5)]. 5-LO was further purified by being passed through a HiLoad Superdex-75 size-exclusion column (Amersham), equilibrated with buffer B. The elution profile exhibited two well-separated major protein peaks, both of which were identified as 5-LO by SDS−PAGE and immunoblot analysis (Figure 1A). The second peak, corresponding to longer retention times, showed profoundly higher lipoxygenase activity than the first peak. The second peak was pooled, transferred to buffer C [150 mM NaCl, 0.1 mM EGTA, and 50 mM Tris-HCl (pH 7.5)], and used immediately for activity experiments. Alternatively, pure distilled water was used in the desalting column, followed by lyophilization and storage at −80 °C for biophysical experiments. The activity of the lyophilized 5-LO sample was sustained at the level of 60−80% over a period of 1 week under these conditions.

The SDS gels were either stained by Coomassie for protein detection or transferred to Hybond ECL membranes (Amersham) for Western blotting. Transfer was accomplished using a Bio-Rad transfer device for 1 h at a constant voltage of 90 V. After the gel had been transferred, the membrane was blocked with 20 mM Tris-HCl, 137 mM NaCl, and 0.1% Tween 20 (pH 7.6) (TBST) containing 7% nonfat dry milk, for 1 h, washed, and incubated with the anti-human 5-LO antibody for 1 h in 1% milk in TBST at room temperature. The membrane was washed four times with 10 mL of 1% milk in TBST and exposed to a horseradish peroxidase-conjugated anti-rabbit secondary antibody (Jackson Immunochemicals) in a similar way. The blot was visualized by using an HRP Super Signal Kit (Pierce) and exposed to Blue Sensitive X-ray film (Midwest Scientific).

5-LO Activity Assay. The 5-LO activity assay buffer [31.64 mM Na_2HPO_4, 5.4 mM KH_2PO_4, 0.2 mM ATP, 0.1 mM dithiothreitol, 0.1 mM EDTA, and 0.3 mM $CaCl_2$ (pH 7.5)] was prepared fresh prior to the assay. Most activity assays were carried out in the presence of large unilamellar lipid vesicles at a total lipid concentration of 0.35 mM, which was shown to support maximum activity of 5-LO. Appropriate volumes of AA in ethanol were aliquoted into glass vials; the solvent was evaporated under nitrogen, and the lipid vesicle suspension in the assay buffer was added to dry AA and gently vortexed. Equal volumes (250 μL) of AA-containing and blank (i.e., without AA) suspensions were used in quartz cuvettes with a path length of 4 mm as sample and reference, respectively. The time scans were recorded on a Cary 100 double-beam spectrophotometer (Varian) at 238 nm. The AA oxygenation reaction was initiated by adding 10 μL of 5-LO in buffer C to the sample cuvette. The specific activity of 5-LO was measured using the initial slope of the kinetic curves of 5-HPETE accumulation, as detected by absorption at 238 nm, using an extinction coefficient of 23 000 M^{-1} cm^{-1} (*44*, *48*) and the final 5-LO concentration in the cuvette. Protein concentrations were measured by the Bradford assay (*49*).

Atomic Absorption Spectroscopy. The iron content in 5-LO samples was determined using a SpectrAA-20 atomic absorption spectrometer equipped with a graphite furnace atomizer (Varian). The 5-LO sample was prepared by dissolving the pure, lyophilized protein in deionized water at a concentration of 13.9 μg/mL (0.178 μM). The instrument was run using an atomizing temperature of 2300 °C, and absorption was measured at 248.3 nm using a spectral band-pass of 0.2 nm. The calibration curve was obtained using appropriate dilutions of a 1000 ppm Fisher certified reference iron solution.

Circular Dichroism Measurements. Circular dichroism (CD) spectra of the protein samples were recorded using a J-810 spectrofluoropolarimeter (Jasco Corp., Tokyo, Japan). This particular instrument has a fluorescence attachment with its photomultiplier mounted at a right angle to the incident light beam and can work at various modes. Protein samples were prepared in a buffer containing 0.1 mM EGTA, 0.3 mM $CaCl_2$, and 50 mM Tris-HCl (pH 7.6) at a concentration of 0.1 mg/mL. Experiments were performed using a quartz cuvette with an optical path length of 0.2 mm, and the temperature was adjusted to 22 °C with a Peltier temperature controller. Ten scans were averaged between 260 and 190 nm and corrected for the background signal by subtracting the spectra of the appropriate control samples without protein. The mean residue molar ellipticity, [θ], was calculated as

$[\theta] = \theta_{meas}/(cn_{res}l)$, where θ_{meas} is the measured ellipticity in millidegrees, c is the molar concentration of the protein, n_{res} is the number of amino acid residues in the protein, and l is the optical path length in millimeters. The α-helical content in proteins was calculated as described previously (*50*, *51*): $f_H = ([\theta]_{222} - [\theta]_u)/([\theta]_H - [\theta]_u)$, where $[\theta]_{222}$ is the experimental mean residue molar ellipticity at 222 nm and $[\theta]_H$ and $[\theta]_u$ are the ellipticities at 222 nm for a totally α-helical and an unordered protein, respectively. The values of the latter two parameters are functions of temperature and the number of residues in the α-helix, n_H: $[\theta]_H = (250T - 44\,000)(1 - 3/n_H)$ and $[\theta]_u = 2220 - 53T$, where T is the temperature in degrees Celsius. Using the structure of rabbit reticulocyte 15-LO (PDB entry 1LOX), we determined that the average number of residues in helices that make at least one turn was 11.4 ± 5.8. Therefore, we used an n_H of 11.4 and an estimated $[\theta]_H$ of −28368.

Preparation of Large Unilamellar Vesicles. Appropriate amounts of lipid stock solutions in chloroform were mixed to obtain desired lipid molar ratios. The solvent was removed under nitrogen, followed by desiccation for ∼3 h. The dry lipids were suspended by being vortexed in appropriate aqueous buffers and were extruded 13 times through two stacked 100 nm pore-size polycarbonate filters using a Liposofast extruder (Avestin, Ottawa, ON) to obtain large unilamellar vesicles.

Fluorescence Measurements. Fluorescence experiments were carried out on the same J-810 spectrofluoropolarimeter, described above, in the fluorescence mode. All experiments were performed using quartz cuvettes with a path length of 0.4 cm, at 22 °C. The excitation and emission slits were adjusted to 4 and 10 nm, respectively. Tryptophans of 5-LO were excited at 290 nm, and the emission was recorded between 300 and 400 nm. Binding of 5-LO to lipid vesicles was assessed by resonance energy transfer (RET) from Trp residues to 1,2-dioleoyl-*sn*-glycero-3-phosphoethanolamine-*N*-(1-pyrenesulfonyl) (Py-PE, 2 mol % in membranes). Lipid vesicles were titrated into a 0.4 μM protein solution, with continuous stirring, to yield a total lipid concentration from 10 to 950 μM. After each addition of vesicles, the sample was equilibrated for 2 min and emission spectra were recorded. Parallel control experiments were conducted with plain vesicles without Py-PE. In control experiments, addition of lipid vesicles caused a slight decrease in the Trp emission intensity as a result of sample dilution. In RET experiments, the Trp fluorescence intensity significantly decreased upon addition of Py-PE-containing vesicles, due to RET from tryptophans of 5-LO to Py-PE in membranes. The fluorescence intensities obtained in RET experiments were corrected for changes in the fluorescence emission as measured in control experiments. The binding data were analyzed using a Langmuir-type formalism (*52*):

$$\Delta F = \Delta F_{max} \frac{[L]}{\frac{1}{K_A} + [L]} \quad (1)$$

where ΔF is the change in the emission intensity at 330 nm at a given lipid concentration relative to the zero lipid level, corrected for the change in intensity when unlabeled lipid was used as control, ΔF_{max} is the saturating level of ΔF calculated by Scatchard plots, and K_A is the binding constant of protein molecules. Binding energies were deduced from binding constants using the relation $\Delta G_A = -RT \ln[W]K_A$, where [W] is the molar concentration of water (55.4 M at 22 °C) and $RT = 0.586$ kcal/mol at 22 °C.

FTIR Measurements. FTIR experiments were performed on a Vector 22 infrared spectrometer (Bruker Optics, Billerica, MA) equipped with a liquid nitrogen-cooled Hg−Cd−Te detector, and a software-operated polarizer (aluminum grid on KRS-5 substrate, Specac, Suffolk, U.K.). Spectra were recorded at 2 cm^{-1} resolution. In direct transmission experiments, the lyophilized protein was dissolved in D_2O-based buffer D [150 mM NaCl, 0.1 mM EGTA, 0.3 mM $CaCl_2$, and 50 mM Tris-HCl (pD 7.6)] and sealed between two CaF_2 windows separated by a 50 μm Teflon spacer, and a series of FTIR spectra were recorded over 3 h. ATR-FTIR experiments were carried out as described previously (*53*). Supported bilayers composed of 1-palmitoyl-2-oleoyl-*sn*-glycero-3-phosphocholine (POPC) were prepared on a germanium internal reflection plate (Spectral Systems, Irvington, NY), using the technique of spreading of sonicated POPC vesicles on top of preformed POPC monolayers. The excess lipid was removed, and at the same time, the solvent was replaced by flushing the cell with 10 volumes of D_2O-based buffer D. 5-LO was dissolved in D_2O-based buffer D and immediately injected into the ATR cell containing the supported membrane, and time-dependent spectra at parallel and perpendicular polarizations were recorded for 3 h. These measurements were used to evaluate the kinetics of membrane binding of 5-LO and the linear dichroism of membrane-bound 5-LO. Comparison of ATR spectra of membrane-bound 5-LO with direct transmission spectra obtained for free 5-LO at similar time points of exposure to D_2O provided information about structural changes in 5-LO induced by membrane binding. The time point of the first exposure of the protein to D_2O was taken as the zero time of amide hydrogen exchange.

RESULTS AND DISCUSSION

Purification and Initial Characterization of 5-LO. 5-LO is known to lose a substantial part of its activity during purification and storage procedures presumably because of exposure to oxygen and subsequent dissociation of the iron cofactor (*47*, *48*, *54*, *55*). In previous studies, the main procedure of 5-LO purification for functional assays was ATP−agarose affinity chromatography, which either was the final step of purification (*44*, *47*, *48*, *54*) or was followed by an additional step of anion-exchange chromatography (*45*, *55*). We have used degassed buffers for 5-LO purification to minimize oxygen-mediated inactivation of the enzyme. The initial procedures that we utilized to purify 5-LO involved precipitation by 50% saturated $(NH_4)_2SO_4$ and ATP−agarose affinity purification, as described previously (*45*, *47*, *48*, *54*, *55*). 5-LO samples purified by these procedures contain appreciable quantities of protein impurities, either 5-LO degradation products or other proteins, as determined by SDS−PAGE (not shown, but see ref *47*). Because our biophysical studies required a highly pure protein, we applied the ATP−agarose-purified 5-LO to a high-resolution HiLoad Superdex-75 size-exclusion column for further purification. The profile of elution from the size-exclusion column exhibited two well-separated protein peaks (Figure 1A), in addition to lower molecular weight proteins

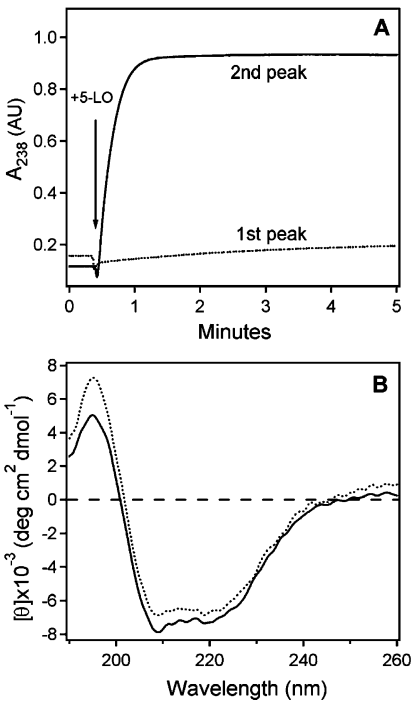

FIGURE 2: Activity and initial structural characterization of the two elution fractions of 5-LO from the Superdex-75 size-exclusion column. (A) Measurements of hydroperoxidase activities of 5-LO from the two elution peaks show little activity of the first peak (···) and high activity of the second peak with a longer retention time (—). In each case, 2.5 μg of enzyme was added to the reaction mixture containing 31.64 mM Na_2HPO_4, 5.4 mM KH_2PO_4, 0.2 mM ATP, 0.1 mM dithiothreitol, 0.1 mM EDTA, 0.3 mM $CaCl_2$, 0.35 mM POPC, and 200 μM AA (pH 7.5). The final 5-LO concentration was 10 μg/mL in both cases. (B) Circular dichroism spectra of the first (···) and second (—) elution peaks of 5-LO from the Superdex-75 column, after correction by subtraction of the spectra of blank buffers. Mean residue molar ellipticities, plotted at the vertical axis, were calculated as described in Experimental Procedures. The buffer consisted of 0.1 mM EGTA, 0.3 mM $CaCl_2$, and 50 mM Tris-HCl (pH 7.6). CD spectra were measured at 22 °C.

(not shown). SDS−PAGE of elution fractions indicated that both major peaks contained a pure $M_r \approx 78$ kDa protein, and the Western blot analysis identified the protein in both peaks as 5-LO (Figure 1B,C).

Measurements of 5-LO activity showed that the first elution peak of 5-LO had little AA hydroperoxidase activity, whereas the second peak, corresponding to longer retention times, exhibited profoundly high lipoxygenase activity (Figure 2A). This clearly shows that 5-LO samples affinity-purified by ATP−agarose resin comprise active and inactive 5-LO fractions, in addition to lower-molecular mass contaminations. Remarkably, the active and inactive 5-LO fractions, which have similar apparent molecular masses in the SDS−polyacrylamide gel, can be separated by size-exclusion chromatography. A possible explanation of this result is that separation by the Superdex column not only occurs on the basis of protein size but also involves a component of protein−resin affinity. The iron-containing 5-LO probably has increased affinity for the resin compared to the iron-deficient fraction.

To characterize the differences between active and inactive fractions of 5-LO, we determined the iron content in both fractions, and compared their far-UV CD spectra. In atomic absorption experiments, we used 5-LO samples from both elution fractions that have been lyophilized from deionized water. These samples were dissolved in deionized water at a concentration of 13.9 μg/mL (0.178 μM), and the absorptions of 10 μL of each solution and of the solvent, atomized at 2300 °C, were measured three to five times each at 248.3 nm. The absorption of the blank solvent was 0.048 ± 0.029, while the absorptions of the inactive and active 5-LO samples were 0.046 ± 0.008 and 0.356 ± 0.07, respectively. The linear part of the calibration curve predicted 0.2 absorption unit per 10 μL of solution containing 6 ng/mL iron. Using the measured absorption intensities, we determined that 5-LO in the first elution peak with negligible activity was essentially devoid of iron, while the sample of the second, active 5-LO fraction contained 10.68 μg/mL (0.191 μM) iron, i.e., 1.07 iron atoms per 5-LO molecule.

Given the fact that LO activity is based on the oxidation−reduction transitions of the iron cofactor (*47*, *48*), this result unequivocally implies that the poor enzymatic activity of the first elution peak results from a negligible iron content. Our results are in accord with earlier findings that aerobic inactivation of 5-LO causes rapid release of iron, but inactive 5-LO still binds to ATP−agarose columns and can be copurified with the active, iron-containing 5-LO fraction (*48*). Iron deficiency in a fraction of the 5-LO sample might have resulted from the imperfect incorporation of iron into 5-LO during biosynthesis in *E. coli*, or iron might have dissociated from a fraction of 5-LO during purification steps.

Iron deficiency could either result from or cause misfolding of part of 5-LO molecules during expression and purification procedures. To identify structural differences between iron-containing and iron-deficient 5-LO samples, we measured CD spectra of 5-LO fractions. Far-UV CD spectra of both active and inactive 5-LO samples exhibited double minima around 222 and 208 nm (Figure 2B), indicating that the secondary structures of both 5-LO fractions were rich in α-helix (*50*, *51*, *56*, *57*). Using the mean residue ellipticities at 222 nm, $[\theta]_{222}$, we estimated that the α-helical contents were ∼39 and ∼37% in the active and inactive 5-LO samples, respectively. Also, the ratio of ellipticities at 222 and 208 nm, $[\theta]_{222}/[\theta]_{208}$, was subtly lower in the active versus the inactive 5-LO sample. Since a decreased $[\theta]_{222}/[\theta]_{208}$ ellipticity ratio has been related to increased rigidity of α-helices (*58*, *59*), the difference between the CD spectra of active and inactive 5-LO samples may indicate more rigid helices in the active 5-LO protein.

Modulation of 5-LO Activity by Membrane Lipids. There is strong evidence that binding to intracellular membranes *in vivo* or to an artificial lipid membrane *in vitro* is a prerequisite for 5-LO activation (*21*−*30*, *42*−*45*). PC has been shown to be more effective in supporting membrane binding and activation of 5-LO than other lipids, including PE, PG, PS, PI, and DAG (*42*, *43*), and the truncated N-terminal C2-like domain of 5-LO had significantly higher affinity for pure PC than for equimolar PC/PS or PC/PG membranes (*35*). We have studied the effect of membrane lipids on 5-LO activity by using a set of lipids with different polar headgroups, including two zwitterionic diacylglycerophospholipids (POPC and POPE), six acidic diacylglycerophospholipids (POPG, POPS, POPA, PI, PIP, and PIP_2), three sphingolipids (ceramide, cerebroside, and sphingomyelin), two monoacylglycerophospholipids (lyso-PC and lyso-PA), a doubly negatively charged tetraacylglycerophospholipid

Table 1: Effect of the Lipid Composition of Membranes of Large Unilamellar Vesicles on 5-LO Activity[a]

lipid added to POPC	10 mol % guest lipid	20 mol % guest lipid
POPE	0.84 ± 0.07	0.62 ± 0.10
POPG	0.79 ± 0.16	0.76 ± 0.09
POPS	0.76 ± 0.21	0.53 ± 0.14
POPA	0.62 ± 0.13	0.89 ± 0.18
PI	0.48 ± 0.15	0.43 ± 0.17
PIP	0.21 ± 0.06	0.16 ± 0.03
PIP_2	0.30 ± 0.09	0.26 ± 0.13
cardiolipin	0.29 ± 0.11	0.71 ± 0.25
Lyso-PC	0.44 ± 0.06	0.61 ± 0.14
Lyso-PA	0.50 ± 0.08	0.63 ± 0.10
POG	0.54 ± 0.16	0.23 ± 0.09
ceramide	0.20 ± 0.07	0.11 ± 0.04
cerebroside	0.38 ± 0.05	0.16 ± 0.02
sphingomyelin	0.64 ± 0.11	0.53 ± 0.20
cholesterol	0.59 ± 0.12	0.45 ± 0.17

[a] Activities are normalized relative to those measured in the presence of 0.35 mM pure POPC vesicles. Mean values of three measurements of 5-LO activities and standard deviations are presented.

(cardiolipin), a steroid (cholesterol), one diacylglycerol (POG), and a cationic diacylglycerophospholipid (DMEPC). The lipid polar headgroup chemistry and the excess charge were varied over a wide range to test if 5-LO, as a peripheral membrane protein, demonstrates lipid headgroup specificity. In most cases, we used POPC as a host lipid in the membranes of large unilamellar vesicles and added 10 or 20 mol % guest lipids because POPC is an abundant lipid in animal cell membranes, and fractions of individual lipids other than PC and PE are moderate. We did not include lipids with heavily glycosylated headgroups, such as gangliosides, because these lipids occur at the external cell surface or in the bloodstream, but usually not in organellar membranes. The cationic lipid, although not physiological, was included as a biophysical probe to study the effect of membrane electrostatics on 5-LO binding and activity. In some specific cases, as described below, we increased the fraction of the guest lipid to 50 or 100 mol % to analyze the observed effects in more detail.

The results of the dependence of 5-LO activity on the lipid composition of membranes are summarized in Table 1 and Figures 3 and 4. The data of Table 1 show that substitution of the trimethylammonium group of PC with a primary amino group (i.e., replacement of POPC with POPE) considerably inhibits 5-LO, indicating that 5-LO may specifically recognize the phosphocholine headgroups of PC.

Analysis of the data of Table 1 reveals a complex nature of modulation of 5-LO by membrane lipids. Negative lipids inhibit the enzyme activity to different degrees, and in some cases (e.g., lysolipids and cardiolipin), the lipids are more inhibitory at the level of 10 mol % than at 20 mol %. Although all singly negatively charged lipids (POPG, POPS, and PI) at 10−20 mol % inhibit 5-LO activity by 20−60%, the effects of lipids with more than one negative charge per molecule are more complex. Interestingly, triply phosphorylated PIP_2 was a weaker inhibitor than the doubly phosphorylated PIP. Probably not only the headgroup excess charge but also the molecular structure of membrane lipids is an important factor for 5-LO activation upon membrane binding. For example, stronger inhibition of PIP than of PI may be electrostatically determined, i.e., may result from impaired interaction of 5-LO with more negatively charged, PIP-containing membranes. On the other hand, the increase

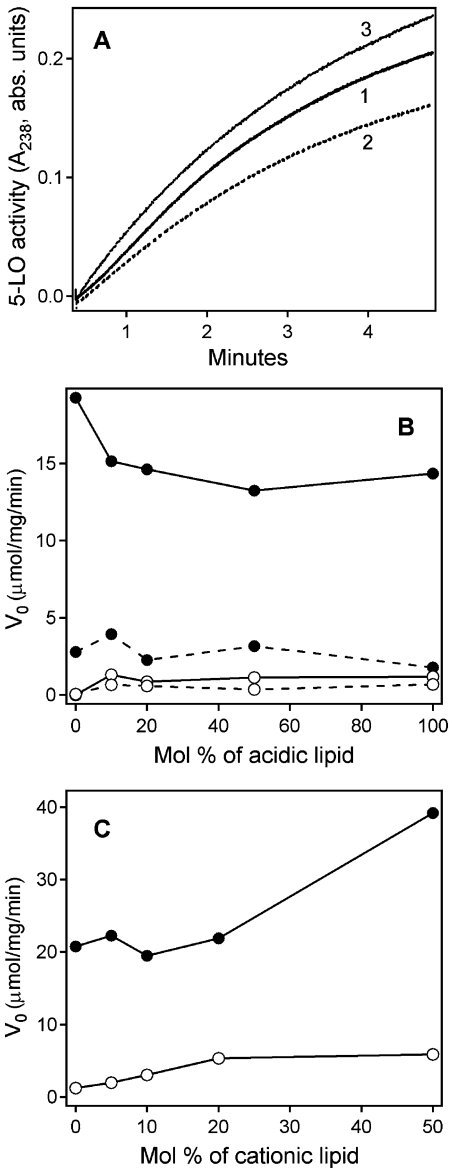

FIGURE 3: Dependence of 5-LO activity on lipid and Ca^{2+} concentrations and on membrane surface charge. (A) Time dependence of the absorption at 238 nm, resulting from 5-LO-catalyzed hydroperoxidation of AA, after addition of 5-LO to lipid suspensions in a buffer containing 31.64 mM Na_2HPO_4, 5.4 mM KH_2PO_4, 0.2 mM ATP, 0.1 mM dithiothreitol, 0.1 mM EDTA, 0.3 mM $CaCl_2$, and 200 μM AA (pH 7.5). Large unilamellar vesicles in the assay buffers were composed of pure POPC (1) or supplemented with 50 mol % anionic POPG (2) or cationic DMEPC (3) at a total lipid concentration of 350 μM. (B) Dependence of the initial velocity of 5-HPETE production, V_0, on the fraction of acidic lipid, POPG, in vesicles: (—) 350 μM total lipid, (− − −) 35 μM total lipid, (●) 0.2 mM free Ca^{2+}, and (○) no free Ca^{2+}. (C) Dependence of V_0 on the fraction of a cationic lipid, DMEPC, in POPC vesicles, in the absence (○) and presence of 0.2 mM free Ca^{2+} (●) at a total lipid concentration of 350 μM.

in 5-LO activity upon replacement of PIP with PIP_2 with a higher negative charge may result from specific affinity of 5-LO for PIP_2. The fact that 10 mol % cardiolipin inhibits 5-LO more than 20 mol % cardiolipin may be ascribed to a decreased packing order of the membrane at higher cardiolipin content (*60, 61*), resulting in easier access of 5-LO to membrane-embedded AA.

Further analysis of the data of Table 1 indicates that all sphingolipids inhibit 5-LO activity. It is remarkable that even

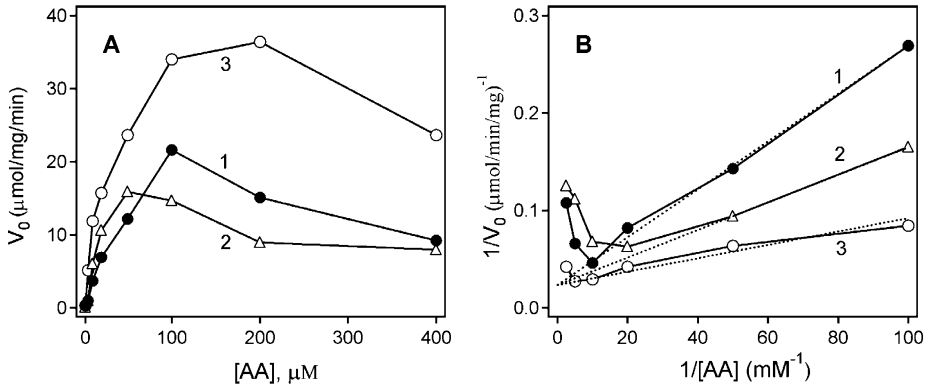

FIGURE 4: (A) Initial velocity of 5-HPETE production, V_0, as a function of AA concentration in the presence of large unilamellar vesicles composed of 100% POPC (1), equimolar POPC and POPG (2), or equimolar POPC and DMEPC (3). The buffer is described in the legend of Figure 3. The total lipid concentration was 350 μM. (B) Double-reciprocal plots of curves presented in panel A, with an AA concentration between 400 and 10 μM. The symbols and numbers corresponding to each curve are the same as in panel A. The dotted lines are linear extrapolations of the curves in the region of low AA concentrations.

sphingomyelin, which has the same phosphocholine headgroup as PC, is inhibitory. Comparison of the effects of the three sphingolipids that were tested shows that their inhibitory effects increase in the following order: sphingomyelin < cerebroside < ceramide. This may indicate that the amide group of sphingolipids itself inhibits 5-LO function. Conversion of ceramide to cerebroside by addition of a pyranosyl residue may mask the amide linkage and weaken the inhibitory effect of ceramide, while the presence of a phosphocholine group in sphingomyelin evidently has a stimulatory effect, as in the case of PC.

It is interesting to note that in most cases inhibition of 5-LO activity by guest lipids cannot be interpreted in terms of a "neutral diluent" effect. For example, POG, cerebroside, and cardiolipin at only 10 mol % inhibit 5-LO by ~50, 60, and 70%, respectively. It is likely that the presence of a particular lipid in membranes affects more than one physical parameter, e.g., membrane surface excess charge and lipid packing order. Certain lipids may also be involved in specific interactions with 5-LO. At each lipid proportion, one factor or the other may be dominant, leading to a nontrivial pattern of the overall effect of lipids on 5-LO activity.

The relatively high concentration of AA (200 μM) that was used in most activity assays might have affected the lipid phase state. To test this conjecture, the lipid packing order in membranes was determined as a function of AA concentration, using the generalized polarization (GP) of a fluorescent membrane probe, 6-lauroyl-2-(*N*,*N*-dimethylamino)naphthalene (Laurdan). We have used POPC as a host lipid and lipids of distinct chemical properties as guest lipids, i.e., 20 mol % additions of an acidic lipid (POPS), a cationic lipid (DMEPC), and a sphingolipid (sphingomyelin). Laurdan (0.5 mol % in membranes) was excited at 360 nm, and its emission spectra were recorded between 390 and 560 nm. The emission spectra of Laurdan are known to shift with an increase in membrane fluidity, resulting in a decrease in GP [$=(I_{435} - I_{500})/(I_{435} + I_{500})$, where I_{435} and I_{500} are the emission intensities at 435 and 500 nm, respectively (*62*−*64*)]. The data (not shown) indicated that GP values of membranes in the absence of AA were in the range of 0.05−0.15 and decreased by less that 0.08 unit in the presence of 200 μM AA. To determine if these changes in GP are indicative of significant changes in the phase state of membranes, we measured the thermotropic phase transition of 1,2-dipalmitoyl-*sn*-glycero-3-phosphocholine (DPPC) by Laurdan GP. The gel-to-liquid-crystalline phase transition of DPPC resulted in a decrease in Laurdan GP from ca. 0.7 to ca. −0.1. This indicates that a significant change in the lipid phase state would correspond to a ΔGP of ≈0.8, while the AA-induced change in GP was less than 0.08. These results indicate that the presence of 200 μM AA does not cause significant changes in the phase state of the membranes. The reason for this is probably that the lipids we used in this study are in the fluid phase and AA cannot make the membranes much more fluid.

Modulation of 5-LO Activity by Membrane Surface Charge and Ca^{2+} Ions. Despite the complex character of the influence of various lipids on 5-LO activity, data summarized in Table 1 demonstrate a trend of suppression of 5-LO activity with an increase in negative surface charge of membranes. To determine if there is a correlation between membrane surface electrostatics and 5-LO activity, we studied the effects of POPG and DMEPC on 5-LO function as anionic and cationic modulators of the membrane surface charge. The kinetic curves presented in Figure 3A demonstrate that in the presence of 350 μM lipid, 200 μM AA, and 0.2 mM free Ca^{2+}, 5-LO activity increases in the presence of membranes containing a cationic lipid, DMEPC, and decreases when the membranes contain anionic POPG. An increase of the fraction of POPG in POPC host membranes at a total lipid concentration of 350 μM and with 0.2 mM free Ca^{2+} causes a decrease in 5-LO activity of ~35% (Figure 3B). Either a 10-fold decrease in lipid concentration or removal of Ca^{2+} results in a strong suppression of 5-LO activity, the effect of Ca^{2+} deprivation being stronger. At low lipid concentrations and in the absence of Ca^{2+}, 5-LO barely exhibits any activity. These data are consistent with previously reported findings that both Ca^{2+} ions and phospholipid membranes are crucial for 5-LO function (*33*, *42*, *43*, *45*, *65*). Although the data of Skorey and Gresser (*44*) suggested that at high lipid concentrations (~350 μM PC) Ca^{2+} is not required for 5-LO activity, Reddy et al. (*45*) have shown that Ca^{2+} considerably increases 5-LO activity at both low and high PC concentrations, which is in line with our results. It has been shown that 70−80% of AA resides in membranes (*43*). In the presence of 200 μM AA, 140−160 μM AA is predicted to distribute into vesicle membranes. The rest of AA (40−60 μM) that stays in the

buffer is likely to be in a monodisperse (nonmicellar) form, because the critical micelle concentration of AA is 73 μM (*66*).

An increase in the fraction of DMEPC in POPC membranes to 50 mol % caused a 2-fold increase in 5-LO activity (Figure 3C). Note, however, that even though removal of Ca^{2+} strongly inhibited 5-LO activity, the level of enzyme activity without Ca^{2+} in the presence of positively charged membranes is severalfold higher than with zwitterionic or acidic membranes (compare panels B and C of Figure 3).

For a better understanding of the effect of membrane surface electrostatics on 5-LO activity, we have analyzed the substrate concentration dependence in the presence of zwitterionic (100% POPC), anionic (50% POPC and 50% POPG), and cationic membranes (50% POPC and 50% DMEPC). 5-LO activity, measured as the initial velocity of AA hydroperoxidation, V_0, exhibited an initial increase and a decline at AA concentrations exceeding ~100 μM (Figure 4A). A straightforward interpretation of this behavior is inhibition of the enzyme at high substrate concentrations by the substrate itself, e.g., because of binding of more than one substrate molecule to the enzyme and formation of nonproductive complexes (*67*). The double-reciprocal plots, presented in Figure 4B, demonstrate the characteristic feature of substrate inhibition, with the curves bent upward as they approach the $1/V_0$ axis. Extrapolated linear parts of these plots (dotted lines) were used to calculate V_{max} (k_{cat}) and K_m. All three extrapolated lines cross the $1/V_0$ axis at the same position, corresponding to a V_{max} of ≈43 μmol min^{-1} mg^{-1}, which corresponds to a turnover number k_{cat} of ≈56 s^{-1}. Combination of the V_{max} value with the slopes of the plots then yields the following Michaelis constants (K_m): 103.2, 64.3, and 31.3 μM for pure POPC, POPC/POPG, and POPC/DMEPC membranes, respectively. If K_m is interpreted as a parameter directly related to the enzyme−substrate dissociation constant, then these results would imply a highest affinity of AA for 5-LO in the presence of cationic membranes, followed by acidic membranes, and followed by zwitterionic membranes. Inhibition of 5-LO activity, as well as other LO isoforms, at high substrate concentrations has been reported previously (*33*, *45*, *68*−*70*). The effect of substrate inhibition is interpreted in terms of two (or more) substrate binding sites of the enzyme, one of which is a productive site and promotes catalysis, while the other site binds AA in a nonproductive mode and inhibits the enzyme.

Although the feature presented in Figure 4B resembles competitive inhibition, this mechanism is not likely to account for the observed effects of the membrane surface charge on 5-LO because the lipid molecules cannot compete with AA for binding to the enzyme active center. Instead, it is likely that the membrane acts as a modulator of 5-LO function. The acquisition by 5-LO of the substrate, AA, which predominantly resides in the membrane (*43*), probably depends on the mode of interaction of 5-LO with the membrane. Stronger interaction of the acidic protein with positively charged membranes probably facilitates substrate binding, resulting in higher enzyme activity. This mechanism may account for the increased activity of 5-LO in the presence of cationic vesicles without Ca^{2+} (Figures 3C and 4). Interestingly, the K_m value obtained in the presence of negatively charged membranes is higher than that for cationic membranes but is lower than that measured for zwitterionic membranes. This may be explained by taking into account the presence of Ca^{2+}. Calcium ions likely mediate binding of 5-LO to acidic and zwitterionic membranes, but may be less important in association of 5-LO with cationic membranes, which is favored by positive membrane electrostatics. One of the mechanisms of Ca^{2+}-mediated membrane binding of LOs is formation of Ca^{2+} bridges between anionic lipids and acidic amino acid side chains of 5-LO (*32*, *38*), although Ca^{2+}-induced structural changes in the enzyme may also be involved (*35*, *44*). Since Ca^{2+} exhibits stronger affinity for acidic than for zwitterionic membranes (*71*), incorporation of acidic lipids in zwitterionic membranes may facilitate Ca^{2+}-mediated membrane binding of 5-LO and at the same time may cause electrostatic repulsion between the acidic protein and negatively charged membranes. For a more direct interpretation of the effect of membrane surface electrostatics and Ca^{2+} ions on 5-LO activity, we have measured Ca^{2+}-mediated binding of 5-LO to membranes with varying surface charges.

Dependence of 5-LO−Membrane Interactions on Membrane Surface Charge and Ca^{2+} Ions. We studied the effect of Ca^{2+} on binding of 5-LO to vesicle membranes containing zwitterionic, anionic, and cationic lipids, using RET from tryptophans of 5-LO to Py-PE in the membranes. When 5-LO was titrated with unlabeled vesicles, the Trp emission intensity changed due to a combination of two effects, i.e., an increase in the emission intensity following membrane binding of 5-LO and a sample dilution effect (Figure 5A). In the case of titration of 5-LO with Py-PE-labeled vesicles, the Trp emission intensity strongly decreased because of RET from Trp to Py-PE (Figure 5B). Pyrene has a complex absorption profile and can be excited by UV radiation at 290 nm, which was used for Trp excitation. Therefore, we assessed RET on the basis of a decrease in the emission intensity of the energy donor, i.e., Trp residues of 5-LO, and not the increase in the emission intensity of pyrene. Since RET is based on short-range (2.8 nm for the Trp−pyrene pair) dipole−dipole interactions between energy donors and acceptors, the observed effect reflects binding of protein molecules to vesicle membranes.

The binding isotherms, presented in Figure 5C, have been constructed on the basis of the dependence of the decrease in Trp emission intensity on lipid concentration through eq 1, as described previously (*52*). In the absence of Ca^{2+}, binding of 5-LO to POPC and POPC/POPG (1:1) membranes is virtually identical and weak, but the affinity for cationic POPC/DMEPC (1:1) membranes is ~20-fold stronger (see Table 2). On the other hand, 0.2 mM free Ca^{2+} enhances the affinity of 5-LO for acidic and zwitterionic membranes 4−8-fold but has little effect on binding of 5-LO to cationic membranes. The binding of 5-LO to cationic membranes is strong and Ca^{2+}-independent (Figure 5C), but Ca^{2+} significantly enhances 5-LO activity in the presence of membranes, including cationic membranes (Figure 3B,C). These data suggest that binding of 5-LO to cationic membranes is mediated by the positive membrane electrostatics, which supports 5-LO binding in both productive and nonproductive modes. The presence of Ca^{2+} probably increases the fraction of productive-mode binding either by bridging the acidic side chains of 5-LO with the phosphate or carbonyl groups of lipids or by causing exposure of hydrophobic side chains of the protein with their subsequent insertion into the membrane.

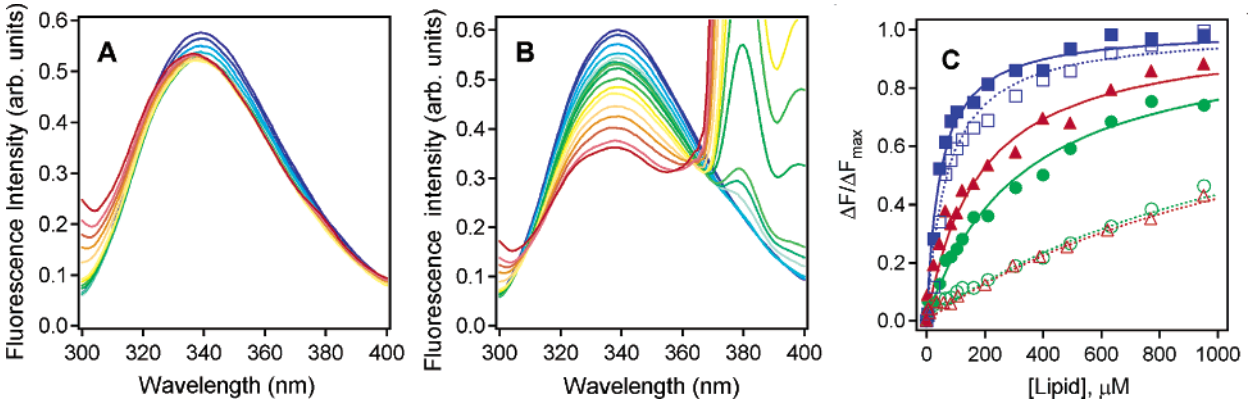

FIGURE 5: (A and B) Representative fluorescence emission spectra of 5-LO with increasing concentrations of vesicles composed of POPC (A) or 98 mol % POPC and 2 mol % Py-PE (B). Tryptophans of 5-LO were selectively excited at 290 nm. In panel A, addition of lipid vesicles causes a slight decrease in the Trp emission intensity as a result of sample dilution, which overcomes the increase in Trp fluorescence due to membrane binding. Spectra in panel B demonstrate a significant decrease in Trp fluorescence intensity due to resonance energy transfer from tryptophans of 5-LO to Py-PE in membranes. The 5-LO concentration was 0.4 μM. The buffer contained 0.1 mM EGTA, 0.3 mM $CaCl_2$, and 50 mM Tris-HCl (pH 7.6). The change in color from blue to red corresponds to a change in lipid concentration from 0 to 950 μM (see panel C). (C) Isotherms characterizing binding of 5-LO to zwitterionic, anionic, and cationic vesicles, constructed on the basis of RET experiments. The relative decrease in Trp fluorescence ($\Delta F/\Delta F_{max}$) upon addition of 2 mol % Py-PE-containing vesicles, due to Trp-to-pyrene RET, was measured, corrected for sample dilution and fluorescence changes in control experiments with unlabeled vesicles, and plotted vs the total lipid concentration. ΔF is the difference between the emission intensity at 330 nm at a given lipid concentration relative to the zero lipid level, and ΔF_{max} is the saturating level of ΔF, determined by Scatchard analysis. The curves were constructed using eq 1: (green) 100% POPC, (red) 50% POPC and 50% POPG, and (blue) 50% POPC and 50% DMEPC and (empty symbols and dotted lines) 0.1 mM EGTA and 50 mM Tris-HCl with no calcium (pH 7.6) and (filled symbols and solid lines) 0.1 mM EGTA, 0.3 mM $CaCl_2$, and 50 mM Tris-HCl (pH 7.6).

Table 2: Binding Constants (K_A) and Binding Energies (ΔG_A) Characterizing the Interaction of 5-LO with Membranes Composed of Various Lipids (binary lipid systems are equimolar) with and without Ca^{2+}, As Indicated

lipid	$[Ca^{2+}]$ (mM)	K_A (M^{-1})	ΔG_A (kcal/mol)
POPC	0.2	3149	−7.07
POPC	0.0	769	−6.25
POPC/POPG	0.2	5624	−7.41
POPC/POPG	0.0	727	−6.21
POPC/DMEPC	0.2	21834	−8.21
POPC/DMEPC	0.0	14478	−7.97

This hydrophobic component, estimated by comparison of the binding energies for DMEPC membranes with and without Ca^{2+}, is only 0.23 kcal/mol (Table 2).

Orientation of 5-LO at the Membrane Surface. We have used polarized ATR-FTIR spectroscopy to characterize the interaction of 5-LO with POPC bilayers supported on a germanium plate. This technique is based on internal reflections of the infrared light inside the plate, which creates an evanescent field at the surface of the plate, where the lipid bilayer and the bound protein reside. Because of the exponentially decaying evanescent field strength, only membrane-bound protein molecules, but not those in the bulk aqueous phase far from the membrane, contribute to the ATR-FTIR absorption spectrum (*53*, *72*). Following injection of 5-LO into the ATR sample cell with a supported POPC bilayer, a prominent amide I band in the 1700−1600 cm^{-1} region appeared, indicating binding of 5-LO to the bilayer. To characterize the kinetics of membrane binding of 5-LO, the amide I area was monitored as a function of time. First, the spectra at parallel and perpendicular polarizations of the infrared light were used to obtain a corrected, polarization-independent spectrum by multiplying the perpendicular spectrum by 0.8 and adding to the parallel spectrum ($A = A_{||} + 0.8A_{\perp}$), as described previously (*73*). After correction, amide I areas were calculated between 1700 and 1563 cm^{-1}

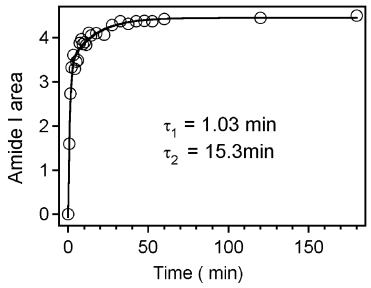

FIGURE 6: Dependence of the amide I area of 5-LO as a function of time after injection of 5-LO into the ATR cell. Amide I areas were calculated between 1700 and 1563 cm^{-1}, after correction of the spectra according to the relation $A = A_{||} + 0.8A_{\perp}$ (see the text for an explanation). The data points have been fitted with a double-exponential function, which yields slow and faster components for the kinetics of membrane binding of 5-LO, as indicated. The buffer consisted of 150 mM NaCl, 50 mM Tris-HCl, 0.1 mM EGTA, and 0.3 mM $CaCl_2$ in D_2O (pD 7.6).

and plotted versus time after injection of 5-LO into the ATR cell. Fitting of the time dependence of the amide I area with a double-exponential function showed that 5-LO adsorption to supported POPC membranes was characterized by two time constants, with values of ∼1 and ∼15 min (Figure 6).

Figure 7A shows several amide I spectra of 5-LO measured at both parallel and perpendicular polarizations of the infrared light. These spectra were used to derive information about the mode of membrane binding of 5-LO. The orientation of membrane-bound peptides or proteins can be estimated using the ATR dichroic ratio ($R^{ATR} = A_{||}/A_{\perp}$, where $A_{||}$ and $A_{\perp}$ are the absorbance intensities at parallel and perpendicular polarizations, respectively). R^{ATR} is easy to interpret for a membrane-bound peptide with a simple secondary structure, such as a single α-helix, or for a protein that has a global rotational symmetry axis, like β-barrels (*53*, *72*, *74*−*76*). For a relatively large protein with complex structure, like 5-LO, the amide I ATR dichroic ratio can

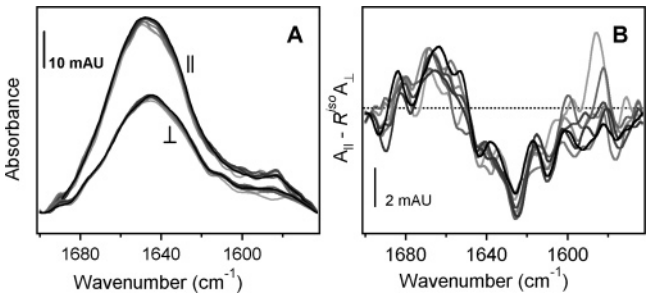

FIGURE 7: (A) Spectra of 5-LO bound to a POPC membrane supported on a germanium plate at parallel and perpendicular polarizations of infrared light, as indicated. The right and left edges of the spectra are at the zero level of absorbance. (B) Corresponding difference spectra calculated according to the relation $A = A_{||} - R^{iso}A_{\perp}$, where $A_{||}$ and $A_{\perp}$ are the spectra measured at parallel and perpendicular polarizations of the infrared light, respectively, with respect to the incidence plane and R^{iso} is the ATR dichroic ratio for an isotropically oriented protein and equals ~1.715 under our experimental conditions (see refs *53* and *73*−*76* for more detail). The dotted line corresponds to the zero level of difference absorbance. The difference spectra ($A = A_{||} - R^{iso}A_{\perp}$) are expected to be flat, at the zero level, for an isotropically oriented protein. Defined and reproducible features of the spectra in panel B demonstrate the nonrandom orientation of 5-LO at the membrane surface. The change in color from light to dark corresponds to the change in time from 17.5 to 60 min after exposure of the protein to D_2O. The buffer is specified in the legend of Figure 6.

hardly be interpreted in a straightforward way because the amide I transition dipoles are likely to adopt an average isotropic orientational distribution. Nevertheless, it is possible to determine if the protein binds to the membrane in a random or defined orientation. In the case of a random, isotropic orientation, $R^{ATR} = R^{iso} \approx 1.715$ (*53*, *73*−*76*), implying that the dependence of the difference ($A_{||} - R^{iso}A_{\perp}$) on the wavenumber will be a horizontal line at the zero level. In the case of a nonrandom, defined orientation, however, it is likely that different secondary structures of the membrane-bound protein adopt distinct orientations with respect to the membrane plane. This will result in positive or negative values of $A_{||} - R^{iso}A_{\perp}$ at certain amide I regions, depending on the orientations of the respective secondary structures. The difference spectra of Figure 7B indicate that $A_{||} - R^{iso}A_{\perp}$ is positive around 1666 cm^{-1} and negative around 1630 cm^{-1}. This feature repeats in all eight spectra and is statistically significant. Taking into account the fact that infrared vibrations around 1630 cm^{-1} are generated by β-sheet structures (see ref *53* and references therein) and that the majority of β-strands of 15-LO are involved in the N-terminal β-barrel (PDB entry 1LOX), one can use the ATR dichroic ratio in this region to evaluate the orientation of the β-barrel axis relative to the membrane normal, using the equation (*74*)

$$\langle 3\cos^2\theta - 1\rangle = \frac{4(E_x^2 - E_y^2 R^{ATR} + E_z^2)}{\left\langle 3\cos^2\left(\frac{\pi}{2} - \beta\right) - 1\right\rangle (E_x^2 - E_y^2 R^{ATR} - 2E_z^2)} \quad (2)$$

where E_x, E_y, and E_z are the orthogonal electric vector components of the evanescent wave and are known entities (*53*, *73*−*76*), θ is the angle between the β-barrel axis and the membrane normal, β is the angle between the strands and the β-barrel axis, and the angular brackets indicate space and time averaging. Inspection of the 15-LO structure shows that the average tilt of the strands relative to the β-barrel axis (β) is ≈20°. Thus, determination of the orientation of the β-barrel of membrane-bound 5-LO (i.e., the angle θ) only requires the ATR dichroic ratio of the β-barrel. As shown in Figure 7B, the difference ($A_{||} - R^{iso}A_{\perp}$) reaches its most negative value of −0.006 at 1626 cm^{-1}, which can readily be ascribed to an amide I mode of a β-sheet (*53*, *75*). However, β-sheet vibrational frequencies occur in a region up to 1635 cm^{-1} (*53*). (Here we do not consider the "higher-frequency component" of antiparallel β-sheets that occur above 1670 cm^{-1}, but are less useful in terms of spectral assignment because of very low extinction coefficients.) The value of the difference $A_{||} - R^{iso}A_{\perp}$ is −0.0028 at 1635 cm^{-1}. By combination of the values of $A_{||} - R^{iso}A_{\perp}$ at 1626 or 1635 cm^{-1} with respective absorbance intensities of parallel polarized spectra (Figure 7A), we determine R^{ATR} equals 1.61 at 1635 cm^{-1} and 1.43 at 1626 cm^{-1}. By inserting these values into eq 2, along with a β of 20°, we determine that the tilt angle θ of the β-barrel axis relative to the membrane normal varies between 39.6 and 49.4°, with an average value of ~45°. Because polarized ATR-FTIR spectroscopy does not distinguish between molecular orientations at angles θ and $\theta \pm 180°$, this finding restricts all possible modes of membrane binding of 5-LO to two mirror image orientations with the β-barrel axis tilted from the membrane normal either by ~45° or by ~45 ± 180°. Combination of this result with earlier findings that tryptophans 13, 75, and 102 of 5-LO (*35*), as well as hydrophobic residues Phe[70], Leu[71], Trp[181], and Leu[195] of rabbit 15-LO, play a major role in membrane anchoring of respective proteins (*37*, *38*), allows one to position the 5-LO molecule at the membrane surface at a unique orientation, because only one of the two mirror image orientations permits physical interactions of these residues with the membrane.

Structural Effects during 5-LO−*Membrane Interactions.* To assess structural changes in 5-LO upon binding to supported membranes, we used difference FTIR spectroscopy. Differences between amide I spectra of the protein under different conditions, e.g., free and membrane-bound, permit identification of spectral changes in the amide I region and interpretation in terms of underlying conformational changes (*53*, *77*). The spectra of Figure 8A show the evolution of the difference between the amide I bands of free and membrane-bound 5-LO, and indicate that the latter spectra are shifted toward lower frequencies. This might reflect more extensive amide H−D exchange of the membrane-bound enzyme, resulting from increased solvent accessibility upon membrane binding. Further analysis of the data shows that this is not the case, however. Data in panels B and C of Figure 8 clearly show that the amide I band of the free enzyme shifts toward higher frequencies during H−D exchange, whereas the spectra of the membrane-bound enzyme do not change appreciably. An increase in the amide I frequency of a protein in D_2O can only be interpreted in terms of conformational changes in the protein, rather than by amide H−D exchange, because amide H−D exchange can only cause a downshift. The increase in absorbance intensity in the 1680−1650 cm^{-1} region accompanied with a decrease in intensity at the low-frequency edge of the amide I region (Figure 8B) is likely to reflect an increase in the

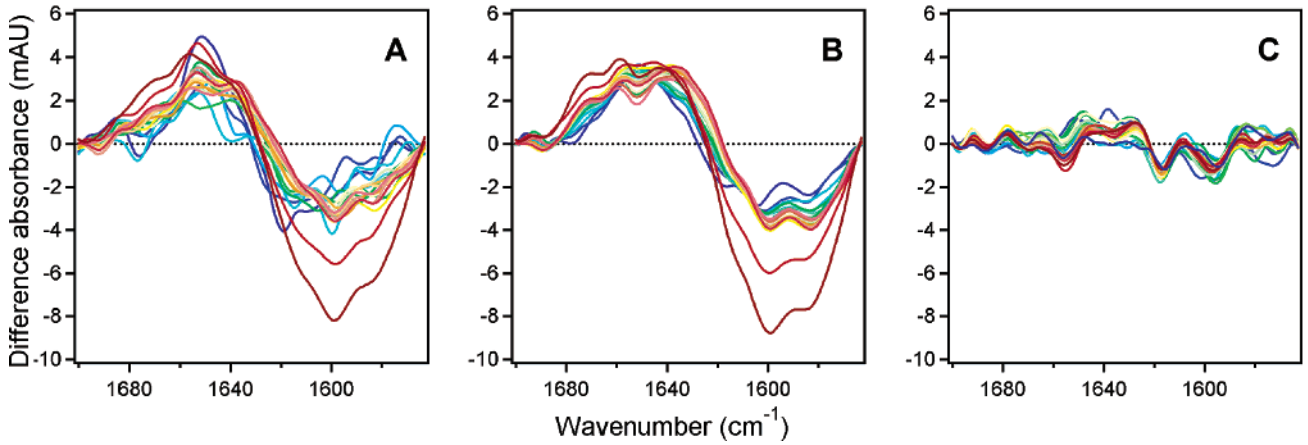

FIGURE 8: Difference FTIR spectra in the amide I region, demonstrating changes in the secondary and dynamic structure of 5-LO free in solution and bound to supported POPC membranes. The lyophilized sample was dissolved in a D_2O-based buffer (see Figure 6) and either sealed between two CaF_2 windows for direct transmission measurements (B) or injected into the ATR cell for ATR-FTIR measurements (C). (A) Difference between spectra of free and membrane-bound 5-LO at similar time points after exposure to D_2O. (B) Progression of spectra of free 5-LO after exposure to D_2O. (C) Progression of spectra of membrane-bound 5-LO after exposure to D_2O (spectra in B and C were obtained according to the relation $A = A_t - A_{3min}$, where A_t is the spectrum at a time point $t > 3$ min). Spectra of the membrane-bound enzyme were measured by the ATR-FTIR technique at parallel and perpendicular polarizations, and corrected according to the relation $A = A_{||} + 0.8A_{\perp}$ (see the text for an explanation). The change in color from blue to burgundy corresponds to the change in deuteration time from 4 min to 3 h (4.2, 5.2, 6.2, 7.2, 8.2, 9.2, 10.2, 11.2, 12.2, 14.2, 17.5, 22.5, 27.5, 32.5, 37.5, 42.5, 47.5, 60, 120, and 180 min).

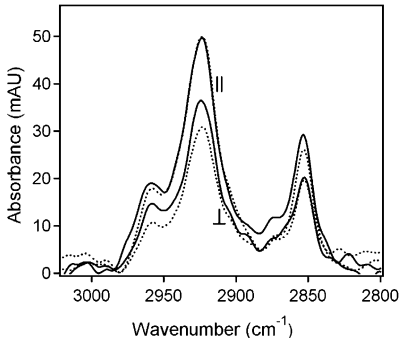

FIGURE 9: Lipid methylene stretching bands of a POPC membrane supported on a germanium plate without (•••) and with bound 5-LO (—), measured after injection of 5-LO for 1 h, at parallel and perpendicular polarizations of the infrared light, as indicated. The supported bilayer was prepared by depositing a POPC monolayer on a germanium plate, by the Langmuir−Blodgett technique, followed by addition of sonicated POPC vesicles, which spread on the monolayer and form the supported bilayer (see Experimental Procedures for more detail). ATR dichroic ratios of POPC without and with bound 5-LO are 1.65 and 1.39, corresponding to lipid acyl chain order parameters of 0.05 and 0.296, respectively.

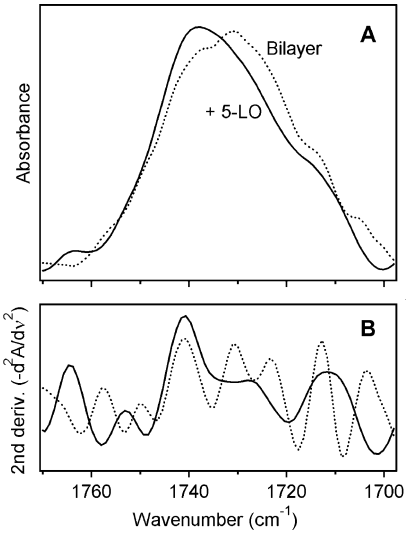

FIGURE 10: (A) ATR-FTIR spectra of the carbonyl stretching vibrations of a POPC membrane supported on a germanium plate without (•••) and with bound 5-LO (—), measured after injection of 5-LO for 1 h. Spectra were measured by the ATR-FTIR technique at parallel and perpendicular polarizations of the infrared light, and corrected according to the relation $A = A_{||} + 0.8A_{\perp}$ (see the text for an explanation). After 5-LO binds, the lipid carbonyl band shifts toward higher frequencies, indicating dehydration of lipid C═O groups. (B) Inverted second derivatives of spectra in panel A. After 5-LO binds, the components around 1731 and 1723 cm^{-1}, corresponding to hydrated lipid C═O groups, disappear, which strongly suggests dehydration of the membrane surface due to 5-LO binding.

fraction of turnlike structures in the protein backbone and alterations of the side chain conformation. Although it is difficult to determine, on the basis of these data, secondary structure elements that convert to turns, it is clear that conformational changes that occur in 5-LO free in the buffer do not occur in the membrane-bound enzyme (Figure 8B,C), implying that membrane binding stabilizes the global protein structure. This result is in line with earlier findings that PC vesicles exerted a stabilizing effect on 5-LO (ref *31* and references therein).

Finally, we have used ATR-FTIR spectroscopy to probe the effect of 5-LO binding on membrane structure and hydration. The spectra of the methylene stretching bands of the supported POPC membrane before and after 5-LO binding indicated a decrease in the lipid dichroic ratio from 1.65 to 1.39 upon 5-LO binding (Figure 9). These values correspond to lipid hydrocarbon chain order parameters of 0.05 and 0.3, respectively (see ref *53* for technical details), indicating that 5-LO binding considerably increases the lipid packing order. Interestingly, the lipid order parameter increased gradually as more 5-LO adsorbed to the membrane. These data, together with those of Figure 8, indicate that the protein−lipid system becomes more ordered as more protein adsorbs to the membrane. Analysis of the spectral shifts in the lipid carbonyl stretching band, which is sensitive to membrane hydration (*53*, *78*, *79*), indicates a shift of the peak of the carbonyl band from 1730.5 to 1737.8 cm^{-1} upon

5-LO binding (Figure 10A). The second derivative of the free bilayer exhibits components at 1740.6, 1730.9, and 1723.2 cm^{-1}. The component at 1740.6 cm^{-1} corresponds to dehydrated carbonyl groups of the lipid, and lower-frequency components are generated by at least partially hydrated C═O groups (*78*, *79*). In the spectrum of the protein-bound membrane, the component at 1740.6 cm^{-1} is preserved, while the lower-frequency components disappear (Figure 10B). This result suggests dehydration of the membrane surface due to 5-LO binding, indicating that the decrease in the entropy of the protein−membrane system due to increased order of the lipids and 5-LO is compensated by the increased entropy of the water component as membrane-bound water is displaced into the bulk phase during 5-LO adsorption.

CONCLUSIONS

In this work, we have improved 5-LO purification protocols, which allows isolation of highly pure and active 5-LO from the inactive, iron-deficient fraction that coelutes with the active fraction from the ATP−agarose affinity column. We have tested the effects of lipid polar headgroups on 5-LO activity, using a wide range of lipids that exist in intracellular membranes, namely, zwitterionic and acidic diacyl- and monoacylglycerophospholipids, sphingolipids, diacylglycerol, and cholesterol. Most lipids had an inhibitory effect on 5-LO activity, while a cationic lipid had a stimulatory effect. The complex pattern of the dependence of 5-LO activity on various lipids indicated that the negative surface charge of membranes is inhibitory, especially in the absence of Ca^{2+}, but is required for Ca^{2+}-mediated membrane binding and activation of 5-LO. Some acidic lipids could facilitate 5-LO activity either by affecting the membrane structure and making accession of membrane-embedded AA easier (cardiolipin) or presumably by specific interactions with 5-LO (PIP_2). The cationic lipid significantly enhanced the affinity of 5-LO for membranes, but its stimulatory effect was relatively modest probably because part of 5-LO binds in a nonproductive mode to positively charged membranes. This may indicate that not only the membrane binding strength but also a proper, productive-mode orientation of the enzyme at the membrane surface is a prerequisite for full enzyme activity. Polarized ATR-FTIR experiments indicated that 5-LO indeed binds to phospholipid bilayers at a defined, nonrandom orientation. We have determined that the β-barrel axis of the N-terminal domain of membrane-bound 5-LO is tilted from the membrane normal by ~45°. This finding, along with previously identified crucial residues for membrane binding of human 5-LO and rabbit 15-LO, allows positioning of the protein molecule at the membrane surface at a unique orientation. Furthermore, our studies show that membrane binding of 5-LO causes dehydration of the membrane surface, and the structures of both membrane lipids and 5-LO become more stable upon their interaction. Our results stress the importance of using quantitative physical approaches to understand molecular events underlying interfacial activation of 5-LO and provide insight in mechanisms of lipid-mediated activation of 5-LO.

ACKNOWLEDGMENT

We thank Prof. Ying-Yi Zhang of Boston University School of Medicine for kindly providing the 5-LO plasmid and Prof. Brooks Madsen of the Department of Chemistry, University of Central Florida, for his help in conducting the atomic absorption spectroscopic experiments.

REFERENCES

1. Kühn, H. (1999) Lipoxygenases, in *Prostaglandins, Leukotrienes, and Other Eicosanoids. From Biogenesis to Clinical Applications* (Marks, F., and Fürstenberger, G., Eds.) pp 109−141, Wiley-VCH, Weinheim, Germany.
2. Brash, A. R. (1999) Lipoxygenases: occurrence, functions, catalysis, and acquisition of substrate, *J. Biol. Chem. 274*, 23679−23682.
3. Feussner, I., and Wasternack, C. (2002) The lipoxygenase pathway, *Annu. Rev. Plant Biol. 53*, 275−297.
4. Oliw, E. H. (2002) Plant and fungal lipoxygenases, *Prostaglandins Other Lipid Mediators 68−69*, 313−323.
5. Rådmark, O. (2002) Arachidonate 5-lipoxygenase, *Prostaglandins Other Lipid Mediators 68−69*, 211−234.
6. Kühn, H., Walther, M., and Kuban, R. J. (2002) Mammalian arachidonate 15-lipoxygenases structure, function, and biological implications, *Prostaglandins Other Lipid Mediators 68−69*, 263−290.
7. Funk, C. D., and Chen, X.-S. (2000) 5-Lipoxygenase and leukotrienes. Transgenic mouse and nuclear targeting studies, *Am. J. Respir. Crit. Care Med. 161*, S120−S124.
8. Rådmark, O. (2003) 5-Lipoxygenase-derived leukotrienes: mediators also of atherosclerotic inflammation, *Arterioscler. Thromb. Vasc. Biol. 23*, 1140−1142.
9. Peters-Golden, M., and Brock, T. G. (2003*)* 5-Lipoxygenase and FLAP, *Prostaglandins, Leukotrienes Essent. Fatty Acids 69*, 99−109.
10. Jonsson, E. W., and Dahlén, S.-E. (1999) The role of eicosanoids in inflammation and allergy, in *Prostaglandins, Leukotrienes, and Other Eicosanoids. From Biogenesis to Clinical Applications* (Marks, F., and Fürstenberger, G., Eds.) pp 233−272, Wiley-VCH, Weinheim, Germany.
11. Ghosh, J., and Myers, C. E. (1999) Central role of arachidonate 5-lipoxygenase in the regulation of cell growth and apoptosis in human prostate cancer cells, *Adv. Exp. Med. Biol. 469*, 577−582.
12. Ghosh, J., and Myers, C. E. (2002) Molecular mechanisms of prostate cancer cell death triggered by inhibition of arachidonate 5-lipoxygenase: involvement of Fas death receptor-mediated signals, *Adv. Exp. Med. Biol. 507*, 415−420.
13. Goodarzi, K., Goodarzi, M., Tager, A. M., Luster, A. D., and von Andrian, U. H. (2003) Leukotriene B4 and BLT1 control cytotoxic effector T cell recruitment to inflamed tissues, *Nat. Immunol. 4*, 965−973.
14. Maccarrone, M., Taccone-Gallucci, M., and Finazzi-Agro, A. (2003) 5-Lipoxygenase-mediated mitochondrial damage and apoptosis of mononuclear cells in ESDR patients, *Kidney Int. Suppl. 84*, S33−S36.
15. Fan, X. M., Tu, S. P., Lam, S. K., Wang, W. P., Wu, J., Wong, W. M., Yuen, M. F., Lin, M. C., Kung, H. F., and Wong, B. C. (2004) Five-lipoxygenase-activating protein inhibitor MK-886 induces apoptosis in gastric cancer through upregulation of p27kip1 and bax, *J. Gastroenterol. Hepatol. 19*, 31−37.
16. Boyington, J. C., Gaffney, B. J., and Amzel, L. M. (1993) The three-dimensional structure of an arachidonic acid 15-lipoxygenase, *Science 260*, 1482−1486.
17. Minor, W., Steczko, J., Stec, B., Otwinowski, Z., Bolin, J. T., Walter, R., and Axelrod, B. (1996) Crystal structure of soybean lipoxygenase L-1 at 1.4 Å resolution, *Biochemistry 35*, 10687−10701.
18. Skrzypczek-Jankun, E., Amzel, L. M., Kroa, B. A., and Funk, M. O., Jr. (1997) Structure of soybean lipoxygenase L3 and a comparison with its L1 isoenzyme, *Proteins: Struct., Funct., Genet. 29*, 15−31.
19. Skrzypczak-Jankun, E., Bross, R. A., Carroll, R. T., Dunham, W. R., and Funk, M. O., Jr. (2001) Three-dimensional structure of a purple lipoxygenase, *J. Am. Chem. Soc. 123*, 10814−10820.
20. Gillmor, S. A., Villaseñor, A., Fletterick, R., Sigal, E., and Browner, M. F. (1997) The structure of mammalian 15-lipoxygenase reveals similarity to the lipases and the determinants of substrate specificity, *Nat. Struct. Biol. 4*, 1003−1009.

21. Rouzer, C. A., and Kargman, S. (1988) Translocation of 5-lipoxygenase to the membrane in human leukocytes challenged with ionophore A23187, *J. Biol. Chem. 263*, 10980−10988.
22. Wong, A., Cook, M. N., Foley, J. J., Sarau, H. M., Marshall, P., and Hwang, S. M. (1991) Influx of extracellular calcium is required for the membrane translocation of 5-lipoxygenase and leukotriene synthesis, *Biochemistry 30*, 9346−9354.
23. Pueringer, R. J., Bahns, C. C., Monick, M. M., and Hunninghake, G. W. (1992) A23187 stimulates translocation of 5-lipoxygenase from cytosol to membrane in human alveolar macrophages, *Am. J. Physiol. 262*, L454−L458.
24. Malaviya, R., Malaviya, R., and Jakschik, B. A. (1993) Reversible translocation of 5-lipoxygenase in mast cells upon IgE/antigen stimulation, *J. Biol. Chem. 268*, 4939−4944.
25. Woods, J. W., Evans, J. F., Ethier, D., Scott, S., Vickers, P. J., Hearn, L., Heibein, J. A., Charleson, S., and Singer, I. I. (1993) 5-Lipoxygenase and 5-lipoxygenase-activating protein are localized in the nuclear envelope of activated human leukocytes, *J. Exp. Med. 178*, 1935−1946.
26. Woods, J. W., Coffey, M. J., Brock, T. G., Singer, I. I., and Peters-Golden, M. (1995) 5-Lipoxygenase is located in the euchromatin of the nucleus in resting human alveolar macrophages and translocates to the nuclear envelope upon cell activation, *J. Clin. Invest. 95*, 2035−2046.
27. Brock, T. G., McNish, R. W., Bailie, M. B., and Peters-Golden, M. (1997) Rapid import of cytosolic 5-lipoxygenase into the nucleus of neutrophils after in vivo recruitment and in vitro adherence, *J. Biol. Chem. 272*, 8276−8280.
28. Brock, T. G., McNish, R. W., and Peters-Golden, M. (1995) Translocation and leukotriene synthetic capacity of nuclear 5-lipoxygenase in rat basophilic leukemia cells and alveolar macrophages, *J. Biol. Chem. 270*, 21652−21658.
29. Brock, T. G., Paine, R., III, and Peters-Golden, M. (1994) Localization of 5-lipoxygenase to the nucleus of unstimulated rat basophilic leukemia cells, *J. Biol. Chem. 269*, 22059−22066.
30. Pouliot, M., McDonald, P. P., Krump, E., Mancini, J. A., McColl, S. R., Weech, P. K., and Borgeat, P. (1996) Colocalization of cytosolic phospholipase A_2, 5-lipoxygenase, and 5-lipoxygenase-activating protein at the nuclear membrane of A23187-stimulated human neutrophils, *Eur. J. Biochem. 238*, 250−258.
31. Rådmark, O. P. (2000) The molecular biology and regulation of 5-lipoxygenase, *Am. J. Respir. Crit. Care Med. 161*, S11−S15.
32. Tatulian, S. A., Steczko, J., and Minor, W. (1998) Uncovering a calcium-regulated membrane-binding mechanism for soybean lipoxygenase-1, *Biochemistry 37*, 15481−15490.
33. Hammarberg, T., Provost, P., Persson, B., and Rådmark, O. (2000) The N-terminal domain of 5-lipoxygenase binds calcium and mediates calcium stimulation of enzyme activity, *J. Biol. Chem. 275*, 38787−38793.
34. Chen, X.-S., and Funk, C. D. (2001) The N-terminal "β-barrel" domain of 5-lipoxygenase is essential for nuclear membrane translocation, *J. Biol. Chem. 276*, 811−818.
35. Kulkarni, S., Das, S., Funk, C. D., Murray, D., and Cho, W. (2002) Molecular basis of the specific subcellular localization of the C2-like domain of 5-lipoxygenase, *J. Biol. Chem. 277*, 13167−13174.
36. May, C., Höhne, M., Gnau, P., Schwennesen, K., and Kindl, H. (2000) The N-terminal β-barrel structure of lipid body lipoxygenase mediates its binding to liposomes and lipid bodies, *Eur. J. Biochem. 267*, 1100−1109.
37. Walther, M., Anton, M., Wiedmann, M., Fletterick, R., and Kühn, H. (2002) The N-terminal domain of the reticulocyte-type 15-lipoxygenase is not essential for enzymatic activity but contains determinants for membrane binding, *J. Biol. Chem. 277*, 27360−27366.
38. Walther, M., Wiesner, R., and Kühn, H. (2004) Investigations into calcium-dependent membrane association of 15-lipoxygenase-1. Mechanistic role of surface-exposed hydrophobic amino acids and calcium, *J. Biol. Chem. 279*, 3717−3725.
39. Bürkert, E., Arnold, C., Hammarberg, T., Rådmark, O., Steinhilber, D., and Werz, O. (2003) The C2-like β-barrel domain mediates the Ca^{2+}-dependent resistance of 5-lipoxygenase activity against inhibition by glutathione peroxidase-1, *J. Biol. Chem. 278*, 42846−42853.
40. Reid, G. K., Kargman, S., Vickers, P. J., Mancini, J. A., Leveille, C., Ethier, D., Miller, D. K., Gillard, J. W., Dixon, R. A., and Evans, J. F. (1990) Correlation between expression of 5-lipoxygenase-activating protein, 5-lipoxygenase, and cellular leukotriene synthesis, *J. Biol. Chem. 265*, 19818−19823.
41. Abramovitz, M., Wong, E., Cox, M. E., Richardson, C. D., Li, C., and Vickers, P. J. (1993) 5-Lipoxygenase-activating protein stimulates the utilization of arachidonic acid by 5-lipoxygenase, *Eur. J. Biochem. 215*, 105−111.
42. Puustinen, T., Scheffer, M. M., and Samuelsson, B. (1988) Regulation of the human leukocyte 5-lipoxygenase: Stimulation by micromolar Ca^{2+} levels and phosphatidylcholine vesicles, *Biochim. Biophys. Acta 960*, 261−267.
43. Noguchi, M., Miyano, M., Matsumoto, T., and Noma, M. (1994) Human 5-lipoxygenase associates with phosphatidylcholine liposomes and modulates LTA4 synthetase activity, *Biochim. Biophys. Acta 1215*, 300−306.
44. Skorey, K. I., and Gresser, M. J. (1998) Calcium is not required for 5-lipoxygenase activity at high phosphatidylcholine vesicle concentrations, *Biochemistry 37*, 8027−8034.
45. Reddy, K. V., Hammarberg, T., and Rådmark, O. (2000) Mg^{2+} activates 5-lipoxygenase in vitro: dependency on concentrations of phosphatidylcholine and arachidonic acid, *Biochemistry 39*, 1840−1848.
46. Zhang, Y.-Y., Rådmark, O., and Samuelsson, B. (1992) Mutagenesis of some conserved residues in human 5-lipoxygenase: effects on enzyme activity, *Proc. Natl. Acad. Sci. U.S.A. 89*, 485−489.
47. Zhang, Y.-Y., Lind, B., Rådmark, O., and Samuelsson, B. (1993) Iron content of human 5-lipoxygenase, effects of mutations regarding conserved histidine residues, *J. Biol. Chem. 268*, 2535−2541.
48. Percival, D. M. (1991) Human 5-lipoxygenase contains an essential iron, *J. Biol. Chem. 266*, 10058−10061.
49. Bradford, M. M. (1976) A rapid and sensitive method for the quantitation of microgram quantities of protein utilizing the principle of protein-dye binding, *Anal. Biochem. 72*, 248−254.
50. Rohl, C. A., and Baldwin, R. L. (1997) Comparison of NH exchange and circular dichroism as techniques for measuring the parameters of the helix-coil transition in proteins, *Biochemistry 36*, 8435−8442.
51. Luo, P., and Baldwin, R. L. (1997) Mechanism of helix induction by trifluoroethanol: A framework for extrapolating the helix-forming properties of peptides from trifluoroethanol/water mixtures back to water, *Biochemistry 36*, 8413−8421.
52. Nalefski, E. A., and Falke, J. J. (1998) Location of the membrane-docking face on the Ca^{2+}-activated C2 domain of cytosolic phospholipase A_2, *Biochemistry 37*, 17642−17650.
53. Tatulian, S. A. (2003) Attenuated total reflection Fourier transform infrared spectroscopy: a method of choice for studying membrane proteins and lipids, *Biochemistry 42*, 11898−11907.
54. Zhang, Y.-Y., Hamberg, M., Rådmark, O., and Samuelsson, B. (1994) Stabilization of purified 5-lipoxygenase with glutathione peroxidase and superoxide dismutase, *Anal. Biochem. 220*, 28−35.
55. Hammarberg, T., and Rådmark, O. (1999) 5-Lipoxygenase binds calcium, *Biochemistry 38*, 4441−4447.
56. Venyaminov, S. Yu., and Yang, J. T. (1996) Determination of protein secondary structure, in *Circular Dichroism and the Conformational Analysis of Biomolecules* (Fasman, G. D., Ed.) pp 69−107, Plenum Press, New York.
57. Kelly, S. M., and Price, N. C. (1997) The application of circular dichroism to studies of protein folding and unfolding, *Biochim. Biophys. Acta 1338*, 161−185.
58. Cooper, T. M., and Woody, R. W. (1990) The effect of conformation on the CD of interacting helices: A theoretical study of tropomyosin, *Biopolymers 30*, 657−676.
59. Zhou, N. E., Kay, C. M., and Hodges, R. S. (1992) Synthetic model proteins. Positional effects of interchain hydrophobic interactions on stability of two-stranded α-helical coiled-coils, *J. Biol. Chem. 267*, 2664−2670.
60. Seddon, J. M. (1990) Structure of the inverted hexagonal (H_{II}) phase, and non-lamellar phase transitions of lipids, *Biochim. Biophys. Acta 1031*, 1−69.
61. Zazueta, C., Ramirez, J., Garcia, N., and Baeza, I. (2003) Cardiolipin regulates the activity of the reconstituted mitochondrial calcium uniporter by modifying the structure of the liposome bilayer, *J. Membr. Biol. 191*, 113−122.
62. Parasassi, T., Di Stefano, M., Loiero, M., Ravagnan, G., and Gratton, E. (1994) Influence of cholesterol on phospholipid bilayers phase domains as detected by Laurdan fluorescence, *Biophys. J. 66*, 120−132.
63. Harris, F. M., Best, K. B., and Bell, J. D. (2002) Use of laurdan fluorescence intensity and polarization to distinguish between

changes in membrane fluidity and phospholipid order, *Biochim. Biophys. Acta 1565*, 123−128.
64. Nyholm, T., Nylund, M., Soderholm, A., and Slotte, J. P. (2003) Properties of palmitoyl phosphatidylcholine, sphingomyelin, and dihydrosphingomyelin bilayer membranes as reported by different fluorescent reporter molecules. *Biophys. J. 84*, 987−997.
65. Hammarberg, T., Reddy, K. V., Persson, B., and Rådmark, O. (2002) Calcium binding to 5-lipoxygenase, *Adv. Exp. Med. Biol. 507*, 17−121.
66. Glick, J., Santoyo, G., and Casey, P. J. (1996) Arachidonate and related unsaturated fatty acids selectively inactivate the guanine nucleotide-binding regulatory protein, G_z, *J. Biol. Chem. 271*, 2949−2954.
67. Schulz, A. R. (1994) *Enzyme Kinetics*, Cambridge University Press, Cambridge, U.K.
68. Egmond, M. R., Brunori, M., and Fasella, P. M. (1976) The steady-state kinetics of the oxygenation of linoleic acid-catalyzed by soybean lipoxygenase, *Eur. J. Biochem. 61*, 93−100.
69. Aharony, D., and Stein, R. L. (1986) Kinetic mechanism of guinea pig neutrophil 5-lipoxygenase, *J. Biol. Chem. 261*, 11512−11519.
70. Werz, O., Bürkert, E., Samuelsson, B., Rådmark, O., and Steinhilber, D. (2002) Activation of 5-lipoxygenase by cell stress is calcium independent in human polymorphonuclear leukocytes, *Blood 99*, 1044−1052.
71. Tatulian, S. A. (1999) Surface electrostatics of biological membranes and ion binding, in *Surface Chemistry and Electrochemistry of Membranes* (Sørensen, T. S., Ed.) pp 871−922, Marcel Dekker, New York.
72. Fringeli, U. P. (1993) *In situ* infrared attenuated total reflection membrane spectroscopy, in *Internal Reflection Spectroscopy* (Mirabella, F. M., Jr., Ed.) pp 255−324, Marcel Dekker, New York.
73. Marsh, D. (1999) Quantitation of secondary structure in ATR infrared spectroscopy, *Biophys. J. 77*, 2630−2637.
74. Marsh, D. (2000) Infrared dichroism of twisted β-sheet barrels. The structure of *E. coli* outer membrane proteins, *J. Mol. Biol. 297*, 803−808.
75. Marsh, D. (1997) Dichroic ratios in polarized Fourier transform infrared for nonaxial symmetry of β-sheet structures, *Biophys. J. 72*, 2710−2718.
76. Marsh, D. (2004) Infrared dichroism of isotope-edited α-helices and β-sheets, *J. Mol. Biol. 338*, 353−367.
77. Gennis, R. B. (2003) Some recent contributions of FTIR difference spectroscopy to the study of cytochrome oxidase, *FEBS Lett. 555*, 2−7.
78. Lewis, R. N., and McElhaney, R. N. (1993) Studies of mixed-chain diacyl phosphatidylcholines with highly asymmetric acyl chains: A Fourier transform infrared spectroscopic study of interfacial hydration and hydrocarbon chain packing in the mixed interdigitated gel phase, *Biophys. J. 65*, 1866−1877.
79. Blume, A., Hübner, W., and Messner, G. (1988) Fourier transform infrared spectroscopy of $^{13}C{=}O$-labeled phospholipids hydrogen bonding to carbonyl groups, *Biochemistry 27*, 8239−8249.

BI048775Y